Research Square

Preprints are preliminary reports that have not undergone peer review.
They should not be considered conclusive, used to inform clinical practice,
or referenced by the media as validated information.

Micropore-Engineered Activated Carbons from Sunflower Pith for Enhanced CO2 Capture

Sahand Saeidi Harzand
Sabanci University
Alp Yürüm
alp.yurum@sabanciuniv.edu

Sabanci University

Research Article

Keywords: Biomass-derived activated carbon, sunflower pith, CO2 capture, KOH activation, NaOH activation, microporosity, pressure swing adsorption

Posted Date: June 22nd, 2026

DOI: https://doi.org/10.21203/rs.3.rs-9936867/v1

License: This work is licensed under a Creative Commons Attribution 4.0 International License.
Read Full License

Additional Declarations: No competing interests reported.

Version of Record: A version of this preprint was published at Adsorption on July 28th, 2026. See the published version at https://doi.org/10.1007/s10450-026-00704-0.

Abstract

Biomass-derived activated carbons are attractive adsorbents for CO_2 capture because they combine low precursor cost, chemical robustness, regenerability, and tunable microporosity. Here, sunflower stem pith, an agricultural residue with a naturally porous cellular structure, was converted into activated carbon by nitrogen carbonization followed by alkali hydroxide activation using either KOH or NaOH. Carbonization temperature and residence time controlled char yield, carbonization degree, and removal of lignocellulosic functional groups, whereas the activation agent governed the final pore architecture. NaOH activation produced the highest BET surface area and total pore volume, with AC-4 reaching 2948 m^2g^{-1}. However, the corresponding KOH-activated carbon, AC-2, showed a lower BET surface area of 2268 m^2g^{-1} but a higher micropore-to-total-pore-volume ratio of 0.78 and a smaller average pore diameter of 2.08 nm. CO_2 adsorption measurements at 25°C up to 8 bar showed that AC-2 delivered the highest uptake, reaching 13.92 mmol g^{-1}, compared with 10.87 mmol g^{-1} for AC-4 and 4.58 mmol g^{-1} for the commercial activated carbon. This inversion between BET surface area and adsorption capacity demonstrates that CO_2 uptake is governed by micropore quality rather than total surface area alone. A confinement-weighted micropore descriptor, defined as micropore volume divided by average pore diameter raised to a fitting exponent, further supported this structure–performance relationship by combining micropore volume and pore-width effects. Temperature-dependent adsorption and isosteric heat analysis confirmed exothermic physisorption, while AC-2 retained 97.8% of its initial uptake after 10 adsorption–desorption cycles under vacuum regeneration. These results establish sunflower pith as a promising agricultural precursor for regenerable CO_2-capture carbons and show that targeted micropore engineering is more important than simple BET surface-area maximization for designing high-performance biomass-derived activated carbons.

1. Introduction

Carbon capture is increasingly recognized as a necessary component of deep-decarbonization strategies, particularly for industrial point sources where direct electrification, feedstock substitution, or complete fuel switching remains technically difficult or economically unrealistic. Cement, iron and steel, petrochemical, refinery, and fossil-fuel-based power systems continue to emit concentrated CO_2 streams, and even aggressive deployment of renewable energy cannot immediately eliminate these process-related emissions. At the same time, global energy-related CO_2 emissions have remained at historically high levels, while the number of announced carbon capture, utilization, and storage projects has increased rapidly in response to net-zero targets and tightening climate policy [1, 2]. These developments highlight a practical materials challenge: carbon capture technologies require adsorbents that are inexpensive, scalable, regenerable, resistant to repeated cycling, and compatible with realistic gas-stream conditions. In this context, the discovery and rational design of robust porous materials from low-cost feedstocks remains a critical research priority.

Among available separation technologies, adsorption using porous solids offers an attractive route for CO_2 capture because it can be integrated into pressure-swing adsorption, vacuum-swing adsorption, or temperature-assisted regeneration processes. Compared with conventional aqueous amine scrubbing, solid adsorbents can reduce corrosion issues, solvent losses, and the large sensible-heat demand associated with heating water-rich absorbent solutions. However, the practical success of adsorption-based capture depends strongly on the balance between CO_2 capacity, selectivity, adsorption kinetics, regeneration energy, and long-term stability. A material with high equilibrium capacity but poor regeneration or slow mass transfer may be unsuitable for cyclic operation. Therefore, effective CO_2 adsorbents must combine strong but reversible CO_2 affinity with a pore architecture that permits rapid uptake and release.

Activated carbons remain among the most realistic solid adsorbents for near-term CO_2 capture applications. They are chemically and thermally stable, mechanically robust, relatively hydrophobic compared with many polar inorganic adsorbents, and can be produced from abundant carbon-rich precursors using established thermal and chemical activation routes [3–6]. Their performance is also highly tunable: by changing the precursor, carbonization conditions, activation agent, activation temperature, and impregnation ratio, the pore volume, pore-size distribution, surface functional groups, and mineral content can be substantially modified. This tunability is especially important because CO_2 adsorption on activated carbons is not controlled by BET surface area alone. Recent studies and reviews on biomass-derived activated carbons emphasize that CO_2 uptake depends on the accessibility and size distribution of micropores, the fraction of ultramicropores, the presence of wider transport pores, surface heteroatom chemistry, ash-derived inorganic species, and the reversibility of adsorption during cycling [3–6].

For CO_2 capture at low to moderate pressures, narrow micropores and ultramicropores are particularly important. When the pore width approaches the kinetic dimension of CO_2, adsorption potentials from opposing pore walls overlap, producing stronger confinement and enhanced CO_2 affinity [7]. This is why pores below approximately 0.7-1.0 nm are often considered especially beneficial for low-pressure CO_2 adsorption. Nevertheless, a carbon structure composed only of extremely narrow pores is not necessarily ideal for all capture conditions. At elevated pressure, wider micropores can provide additional capacity, while narrow mesopores can facilitate gas transport and improve access to internal adsorption sites. Therefore, high-performance activated carbons should not be designed simply by maximizing total surface area. Instead, the goal should be to generate a well-balanced pore network in which ultramicropores provide strong affinity, micropores contribute high adsorption capacity, and small mesopores support diffusion and cyclic working performance.

The choice of biomass precursor is another important factor because it determines both the sustainability and the final pore architecture of the activated carbon. Agricultural residues offer an appealing platform for producing low-cost adsorbents because they are renewable, geographically distributed, and often underutilized. Converting such residues into activated carbons can simultaneously

reduce waste-disposal burdens and create value-added materials for environmental applications. However, biomass precursors differ substantially in their lignocellulosic composition, inorganic content, density, morphology, and thermal decomposition behavior. These differences influence char yield, carbonization degree, reactivity toward chemical activating agents, ash formation, and pore evolution during activation. Therefore, each biomass source requires specific evaluation rather than assuming that all lignocellulosic residues behave similarly.

Sunflower pith is a particularly interesting precursor in this regard. It is a lightweight, foam-like internal stem material with a naturally porous cellular morphology. Such a structure may facilitate chemical penetration during activation and promote the formation of an interconnected carbon framework. Sunflowers are also widely cultivated, and their stem residues are generally low-value agricultural byproducts. Previous studies on sunflower-pith-derived carbons have shown that high-surface-area activated carbons can be obtained and used for adsorption applications [8]. However, the relationship between the activating agent, carbon pore architecture, and CO_2 adsorption behavior has not been clarified in sufficient detail for this precursor. In particular, it remains important to determine whether superior CO_2 uptake is primarily associated with total BET surface area, total pore volume, micropore fraction, or more subtle differences in pore-size distribution.

In this work, sunflower pith is investigated as a sustainable agricultural residue for the preparation of activated carbons for CO_2 capture. Activated carbons were produced by carbonization followed by chemical activation, and KOH and NaOH were compared as activating agents to clarify how alkali chemistry influences pore development and adsorption performance. This comparison is scientifically important because both hydroxides can generate highly porous carbons, but they do not necessarily produce equivalent pore-size distributions or CO_2-accessible micropore structures. By comparing the textural properties and CO_2 adsorption behavior of the resulting carbons, this study separates the effect of total surface area from the effect of pore architecture.

The central finding is that the highest BET surface area does not correspond to the highest CO_2 uptake. Although NaOH activation produces a carbon with larger total surface area and pore volume, the KOH-activated sample exhibits superior CO_2 adsorption because it develops a more favorable microporous architecture. This result demonstrates that the effectiveness of sunflower-pith-derived activated carbons is governed by the quality of the pore network rather than by surface-area maximization alone. The work therefore contributes to the broader design principle that biomass-derived activated carbons for CO_2 capture should be engineered through targeted micropore control, balancing pore volume, pore diameter, and regeneration stability. By identifying sunflower pith as a viable precursor and clarifying the role of alkali activation chemistry, this study provides a practical and mechanistic basis for developing low-cost, regenerable activated carbons from agricultural residues.

2. Experimental section

2.1 Materials

Sunflower pith was collected as agricultural residue from Düğüncülü village near Kırklareli, northwestern Türkiye. Potassium hydroxide (KOH, Merck KGaA), sodium hydroxide (NaOH, Sigma-Aldrich, 98–100%), hydrochloric acid, and distilled water were used as received. A commercial coal-based activated carbon sample from Merck KGaA was used as a benchmark.

2.2 Carbonization and activation

The dried sunflower stems were peeled, and the inner pith was collected, ground, and sieved to approximately 1 mm particles. The precursor was carbonized under nitrogen at a heating rate of 10°C min^{-1}. Carbonization temperatures of 350, 400, 450, and 500°C and holding times of 30, 60, and 120 min were evaluated. The biochars were labeled BC-1 to BC-12 according to the carbonization matrix Table 1). Based on yield, functional-group removal, and preliminary surface-area results, BC-11 (500°C, 60 min) and BC-12 (500°C, 120 min) were selected for activation (Table 2).

Table 1
Synthesized bio-char labeling

		Carbonization Temperature (°C)			
		350	400	450	500
Duration (min)	30	BC-1	BC-4	BC-7	BC-10
	60	BC-2	BC-5	BC-8	BC-11
	120	BC-3	BC-6	BC-9	BC-12

Table 2
Synthesized bio-char labeling

		Agent	
		KOH	NaOH
Bio-Char	BC-11	AC-1	AC-3
	BC-12	AC-2	AC-4

For chemical activation, each selected biochar was mixed with either KOH or NaOH at an activating-agent:biochar mass ratio of 3:1 in sufficient distilled water to form a slurry. The slurry was stirred for 2 h, dried at 130°C for 4 h, and heated under nitrogen to 700°C at 10°C min^{-1}. After cooling, the activated product was washed with 0.1 M HCl and hot distilled water until the filtrate reached pH 6.5–7.5, then dried at 110°C for 24 h. The final activated carbons were labeled AC-1 (BC-11/KOH), AC-2 (BC-12/KOH), AC-3 (BC-11/NaOH), and AC-4 (BC-12/NaOH).

2.3 Characterization

Nitrogen adsorption-desorption isotherms at 77 K were collected using a Micromeritics 3Flex surface characterization system. BET surface areas were calculated in the appropriate relative-pressure range, recognizing that highly microporous carbons may require restricted BET fitting ranges. Total pore volumes were estimated near P/P_0 = 0.99, micropore volumes were obtained by the Dubinin-Radushkevich method. Thermogravimetric analysis was carried out using a NETZSCH STA 449 C Jupiter instrument at 10°C min^{-1}. FTIR spectra were recorded using a Thermo Scientific Nicolet iS10 spectrometer from 4000 to 500 cm^{-1}. Morphologies were examined by field-emission scanning electron microscopy (Nano SEM 230).

2.4 CO_2 adsorption and thermodynamic analysis

CO_2 adsorption isotherms were recorded gravimetrically using a Hiden Isochema IGA-001 gas sorption analyzer over 0–8 bar at 25°C. The best-performing sample was further tested at 25, 45, and 65°C to evaluate the temperature dependence of adsorption. The isosteric heat of adsorption was estimated with constant surface coverage after constructing the Langmuir surface-coverage plots.

3. Results and discussion

3.1 Carbonization behavior and surface chemistry

Biochar yield decreased systematically with increasing carbonization severity, from 44% for BC-1 carbonized at 350°C for 30 min to 33% for BC-12 carbonized at 500°C for 120 min (Table 3). This decrease reflects the progressive conversion of sunflower pith from an oxygen-rich lignocellulosic material into a carbon-rich char through dehydration, hemicellulose/cellulose decomposition, cleavage of aliphatic and ether linkages, decarboxylation/decarbonylation, and release of H_2O, CO, CO_2, light hydrocarbons, and tar-forming volatiles. The effect of temperature was more pronounced than residence time, suggesting that the main transformation was controlled primarily by thermal severity in the investigated range. The brownish color of chars prepared at 350–400°C indicates incomplete carbonization and retention of partially decomposed biomass fragments, whereas the black appearance of chars prepared at 450–500°C is consistent with greater aromatization and formation of condensed carbon domains. The simpler TGA combustion profile of the 500°C chars further supports their lower residual volatile content and higher carbonization degree (Figure S1). Similar yield reductions with increasing pyrolysis temperature have been reported for recent biomass-derived chars, where lower solid yield is accompanied by greater fixed-carbon enrichment and improved thermal stability [9–11]. BC-11 and BC-12 were selected for activation because their yield, color, and combustion behavior collectively indicate a suitable balance between carbonization degree and remaining reactivity for subsequent alkali activation.

The FTIR spectra provide direct evidence for the chemical transformation of sunflower pith from an oxygen-rich lignocellulosic precursor into a more condensed carbonaceous structure. The raw sunflower pith exhibited a broad band at 3331 cm^{-1}, assigned to O-H stretching from hydroxyl groups in cellulose,

hemicellulose, lignin, and adsorbed moisture. The band at 2903 cm^{-1} corresponds to aliphatic C-H stretching, while the signals at 1598 and 1416 cm^{-1} indicate aromatic C = C vibrations associated mainly with lignin-derived structures (Figure S2 & Table S1). Additional bands at 1203 and 1022 cm^{-1} are attributed to C-O and C-O-C vibrations from alcohol, ether, and polysaccharide components, confirming the typical chemical signature of a lignocellulosic biomass precursor. Similar oxygenated surface groups, particularly -OH, C = O, and C-O functionalities, have recently been reported for biomass-derived chars and activated carbons prepared from agrifood and lignocellulosic residues [12, 13]. In this sense, sunflower pith behaves as a conventional lignocellulosic precursor, but its low-density pith structure makes it attractive for conversion into porous carbon.

Table 3
Yield percentage for bio-chars (in parentheses)

		Carbonization Temperature (°C)			
		350	400	450	500
Duration (min)	30	BC-1 (44)	BC-4 (40)	BC-7 (38)	BC-10 (35)
	60	BC-2 (43)	BC-5 (39)	BC-8 (37)	BC-11 (34)
	120	BC-3 (41)	BC-6 (37)	BC-9 (36)	BC-12 (33)

With increasing carbonization temperature, the FTIR spectra show a progressive loss of oxygenated and aliphatic functionalities (Fig. 1). The disappearance or strong attenuation of the aliphatic C-H band near 2920 cm^{-1} indicates the removal of hydrogen-rich side chains and volatile fragments during pyrolysis. Similarly, the weakening of C-O and C-O-C bands between approximately 1300 and 1000 cm^{-1} reflects dehydration, depolymerization, and cleavage of cellulose/hemicellulose-derived ether and alcohol groups. This behavior is consistent with recent studies on biomass-derived carbons, where pyrolysis and activation progressively reduce labile oxygen-containing functional groups while increasing the relative contribution of aromatic and condensed carbon domains [12–14]. Therefore, the FTIR results should not be interpreted simply as “functional groups disappeared.” Rather, they indicate the expected chemical maturation of the biomass: oxygen-rich biopolymers are converted into a more thermally stable, carbon-rich char through dehydration, decarboxylation, decarbonylation, and aromatization reactions.

The temperature effect is much more pronounced than the residence-time effect. Chars produced at 350 and 400°C still retain bands associated with O-H, aliphatic C-H, aromatic C = C, and C-O groups, indicating incomplete carbonization and the persistence of partially decomposed biomass fragments. This agrees with the observed brownish color of low-temperature chars, which is typical of incompletely aromatized biomass. By contrast, the chars produced at 450–500°C show much weaker bands in the 3500 – 1600 cm^{-1} region, confirming a higher degree of devolatilization and condensation. This trend is consistent with the known thermal decomposition sequence of lignocellulosic biomass: hemicellulose decomposes at relatively low temperature, cellulose undergoes major depolymerization at intermediate temperature, and lignin contributes to the gradual formation of aromatic carbon structures over a

broader temperature range. Recent biochar studies similarly report that higher carbonization temperatures increase carbon ordering while decreasing the intensity of FTIR bands associated with labile oxygenated and aliphatic groups [3].

The remaining bands after carbonization are also meaningful. The persistence of aromatic C-H deformation bands near 860–870 cm^{-1} suggests that the carbonized sunflower pith still contains substituted aromatic domains rather than a fully graphitized structure. This is expected because the carbonization temperature used here is moderate. Such partially aromatized chars are generally suitable for chemical activation because they retain enough structural reactivity for alkali-assisted bond cleavage, gasification, and pore development during the subsequent activation step. In other words, the 500°C carbonization step produces an activation-ready char: the precursor is sufficiently carbonized to remove unstable biomass fragments, but not so over-condensed that it becomes chemically inert toward KOH or NaOH activation.

After alkali activation at 700°C, the FTIR spectra of the activated carbons become considerably simpler (Fig. 2). The disappearance of the aliphatic deformation band near 1400 cm^{-1} indicates further removal of residual hydrogen-containing organic fragments during activation. The activated carbons mainly retain bands assigned to C = O stretching, C-O-C stretching, and aromatic C-H vibrations. This indicates that chemical activation does not merely “clean” the surface; it restructures the carbon matrix while leaving a limited population of oxygen-containing groups at defect sites, edges, and pore walls. Recent KOH-activated biomass carbon studies also report that activation changes both the carbon framework and surface chemistry, with FTIR commonly showing residual C-O and C = O groups after high-temperature treatment [13–15]. These oxygen-containing groups can contribute to local surface polarity, which may improve interaction with quadrupolar CO_2 molecules, although their contribution should be considered secondary to the pore-structure effects that will be discussed later in the text [3, 15].

The comparison between KOH- and NaOH-activated samples should therefore be discussed carefully at this stage. FTIR does not show a fundamentally different surface chemistry for the two activation agents; instead, both treatments produce activated carbons with broadly similar residual oxygenated and aromatic signatures. This means that the superior CO_2 uptake of the KOH-activated samples should not be attributed to a unique FTIR-detectable functional group. The FTIR results mainly show that both alkali hydroxides effectively remove most lignocellulosic functionalities and convert the sunflower pith char into a chemically matured carbon framework. The difference between KOH and NaOH is expected to arise more strongly from the way each agent develops the pore network during activation, rather than from major differences in surface functional groups detectable by FTIR. This distinction is important because recent CO_2-capture studies on biomass-derived activated carbons increasingly emphasize that surface oxygen groups may enhance local CO_2 affinity, but adsorption capacity is usually governed by the combined effect of surface chemistry and accessible narrow microporosity [3, 15].

Overall, the FTIR results confirm a stepwise chemical transformation: raw sunflower pith contains abundant hydroxyl, aliphatic, aromatic, and ether/alcohol groups typical of lignocellulosic biomass;

carbonization progressively removes labile oxygenated and aliphatic functionalities while promoting aromatization; and alkali activation further simplifies the surface chemistry, leaving mainly aromatic carbon with residual oxygen-containing edge groups. Thus, the role of carbonization is not only to reduce mass or remove volatiles, but to chemically prepare the sunflower pith structure for controlled alkali activation. This interpretation is consistent with recent biomass-derived activated carbon literature, where the most effective CO_2 sorbents are obtained not by preserving the original biomass chemistry, but by converting it into a stable carbon framework with a controlled balance of residual polar groups and activation-developed microporosity [3, 13, 15].

3.2. Textural properties and activation-agent effect

Nitrogen sorption analysis shows that chemical activation transformed the selected sunflower-pith biochars into highly porous activated carbons with strongly developed micro/mesoporous structures (Fig. 3 & Table 4). All biomass-derived activated carbons exhibited much higher textural development than the commercial activated carbon, but the pore architecture depended strongly on the activating agent. The KOH-activated samples, AC-1 and AC-2, gave BET surface areas of 2109 and 2268 $m^2 g^{-1}$, respectively, whereas the NaOH-activated samples, AC-3 and AC-4, reached still higher values of 2658 and 2948 $m^2 g^{-1}$. At first glance, this suggests that NaOH is the more aggressive activating agent for sunflower-pith char. However, the pore-volume distribution shows a more important distinction: KOH activation produced a higher fraction of micropore volume, while NaOH activation generated larger total pore volume but also a greater contribution from wider pores. AC-2, for example, had a micropore/total pore-volume ratio of 0.78 and an average pore diameter of 2.1 nm, whereas AC-4 had a lower micropore fraction of 0.68 and a larger average pore diameter of 2.6 nm. Therefore, NaOH activation maximized apparent surface area and total pore volume, while KOH activation better preserved a narrow-pore architecture.

Table 4
Textural properties of the activated samples

Sample	*BET area ($m^2 g^{-1}$)*	*V_{total} ($cm^3 g^{-1}$)*	*V_{micro} ($cm^3 g^{-1}$)*	*V_{meso} ($cm^3 g^{-1}$)*	*V_{micro}/V_{total}*	*Avg. pore diameter (nm)*
AC-1	***2109***	***0.91***	***0.69***	***0.22***	***0.75***	***2.2***
AC-2	***2268***	***1.09***	***0.83***	***0.26***	***0.78***	***2.1***
AC-3	**2658**	**1.21**	**0.88**	**0.33**	**0.69**	**2.9**
AC-4	**2948**	**1.56**	**1.07**	**0.49**	**0.68**	**2.6**
AC-COM	**754**	**0.53**	**0.18**	**0.37**	**0.34**	**5.8**

The N_2 adsorption–desorption isotherms support the conclusion that alkali activation produced a combined micro–mesoporous pore network. All sunflower-pith-derived activated carbons showed a

sharp uptake at low relative pressure, which is consistent with micropore filling, followed by continued N_2 adsorption at higher relative pressure, indicating additional contribution from wider micropores and/or mesopores. Similar combined Type I/Type IV features have been reported for waste-biomass-derived activated carbons, where the authors assigned this behavior to the coexistence of micropores and mesopores [16]. The development of such hierarchical porosity is strongly affected by activation chemistry and processing conditions. For example, recent studies on biomass-derived activated carbons show that activation temperature, impregnation ratio, and the selected chemical activating agent can shift the pore structure from predominantly microporous to broader micro–mesoporous networks [15, 17]. In the present case, sunflower-pith char was highly responsive to alkali activation: even the lowest-surface-area synthesized sample, AC-1, showed a much higher BET surface area and micropore fraction than the commercial activated carbon. This confirms that the selected biomass precursor and alkali-activation route are effective for producing highly porous carbon adsorbents, while the KOH/NaOH comparison shows that total surface area and micropore fraction must be evaluated separately.

The textural differences between the KOH and NaOH-activated samples can be understood from the coupled chemical and structural processes that occur during high-temperature alkali activation. Alkali hydroxide activation is not a simple surface-cleaning treatment; it involves penetration of hydroxide-derived species into the carbonized framework, reaction with residual oxygenated groups and defect-rich carbon domains, partial gasification/oxidation of the carbon matrix, formation of alkali carbonates/oxides, and removal of inorganic residues during the washing step. For KOH activation, the commonly described mechanism involves conversion of KOH to K_2O, reduction to metallic potassium, intercalation of potassium into the carbon lattice, expansion of graphene-like/turbostratic layers, and simultaneous carbon oxidation to CO, CO_2, and K_2CO_3, all of which contribute to pore formation [15]. Earlier mechanistic studies comparing NaOH and KOH activation also showed that the final porosity depends strongly on the hydroxide used, carbon precursor, reaction atmosphere, and chemical state of the activating agent, confirming that hydroxide activation is a precursor-dependent chemical reaction rather than a universal physical pore-opening process [18].

The response of the sunflower-pith char should therefore be interpreted as a precursor–activator interaction. Carbonization at 500°C is expected to produce a disordered, turbostratic carbon framework composed of small aromatic domains, edge defects, residual oxygenated groups, and accessible voids inherited from the low-density pith structure. Such a framework is reactive toward alkali hydroxides because defect sites and oxygen-containing groups can initiate carbon–alkali reactions, while interlayer gaps and partially open pores allow molten or mobile alkali-derived species to penetrate the char. Under the activation conditions used here, NaOH produced lower activated-carbon yields, higher BET surface areas, larger total pore volumes, larger mesopore volumes, and larger average pore diameters than KOH. This combination indicates that NaOH caused more extensive carbon consumption and pore widening in the sunflower-pith framework (Fig. 4). A recent NaOH/KOH comparison on wood-derived carbons gives a chemically relevant explanation: NaOH-activated samples had lower oxygen contents than KOH-activated samples, which was attributed to the smaller Na^+ cation penetrating more deeply into the

precursor structure and interacting more actively with oxygen-containing groups [19]. The same study also reported slightly higher N_2 sorption and higher specific surface areas for NaOH-activated wood carbons than for KOH-activated analogues, and concluded that alkali-activated samples develop bimodal micro/mesoporous pore-size distributions whose structure depends on both carbonization route and activator [19].

In the present sunflower-pith system, this provides a plausible explanation for the observed NaOH behavior. Na-containing species can strongly attack the accessible, oxygen-containing, defect-rich char framework, promoting deeper chemical etching, removal of oxygenated fragments, carbon gasification, and widening of initially narrow pores. This produces a larger total internal surface area, but it also shifts part of the pore network toward wider micropores and mesopores. KOH activation follows a related but not identical pathway. Potassium-derived species are widely associated with intercalation-assisted expansion of disordered carbon layers; metallic potassium generated during activation can penetrate between graphene-like domains and expand the turbostratic structure, while oxidation/gasification reactions generate porosity [15, 18]. In this work, KOH did not maximize BET surface area, but it retained a larger fraction of micropore volume and produced smaller average pore diameters than NaOH. Thus, KOH appears to provide a more micropore-preserving activation pathway for sunflower-pith char, whereas NaOH produces stronger overall pore opening and widening.

This distinction is important for CO_2 capture because adsorption performance is not governed by BET surface area alone. Recent biomass-derived carbon studies for CO_2 capture show that sub-nanometer pores and polar oxygenated surface sites enhance CO_2 affinity, while different activation routes can produce different balances of ultramicroporosity, total pore volume, and surface chemistry [15]. Therefore, the higher BET surface area of the NaOH-activated samples should not automatically be interpreted as a superior CO_2-capture structure. Instead, the present results indicate that NaOH activation overdevelops or widens part of the sunflower-pith pore network, whereas KOH activation gives a more CO_2-relevant micropore-rich architecture. The key mechanistic conclusion is that NaOH and KOH both activate carbon through high-temperature alkali–carbon reactions, but their interaction with the turbostratic sunflower-pith char differs: NaOH promotes stronger framework etching and pore widening, while KOH better preserves narrow microporosity through intercalation-assisted expansion and controlled gasification. This explains why NaOH gives the highest BET surface area, whereas KOH gives the better pore architecture for CO_2 adsorption.

The commercial activated carbon provides a useful benchmark. Its BET surface area was only 754 m^2 g^{-1}, with a total pore volume of 0.53 cm^3 g^{-1}, a micropore volume of 0.18 cm^3 g^{-1}, and an average pore diameter of 5.81 nm. This indicates a much larger contribution from mesopores compared with the sunflower-pith activated carbons. Although mesopores can improve diffusion and mass transfer in practical adsorption beds, they contribute less strongly to equilibrium CO_2 uptake than narrow micropores at moderate pressures. The synthesized biomass-derived carbons therefore offer two advantages over the commercial sample: much larger total accessible surface and, more importantly, a

much higher fraction of microporosity. Recent reviews of biomass-derived activated carbons for CO_2 capture similarly identify micropore volume and pore-size matching as key factors distinguishing high-performing adsorbents from general-purpose commercial carbons [3, 13, 15, 20–23].

The comparison with recent biomass-derived activated carbons further supports the significance of the present materials. Dziejarski et al. reported pine-wood-derived activated carbons prepared using KOH, $K_2C_2O_4$, and combined KOH/$K_2C_2O_4$ activation; their optimized co-activated carbon reached a BET surface area of 2029 $m^2\ g^{-1}$ and a total pore volume of 1.028 $cm^3\ g^{-1}$, while KOH-activated carbon showed high CO_2 uptake due to extensive ultramicropore development [15]. These values are comparable to, or lower than, the textural properties obtained here for sunflower-pith-derived carbons, especially AC-2 and AC-4. A 2026 study on Parrotia persica wood also showed that the selection of activating agent and impregnation ratio strongly controls CO_2/N_2-relevant pore structures, again confirming that precursor–activator matching is central to adsorbent design [24]. Similarly, recent NaOH-activated avocado-seed carbons and KOH-functionalized oil-palm-derived adsorbents show that alkali activation can generate high-surface-area carbons, but the final adsorption performance depends on whether the activation strategy produces CO_2-accessible micropores rather than only high BET area [25, 26].

The pore-size distribution results are therefore central to the mechanistic interpretation of the activation-agent effect. NaOH activation appears to have promoted broader pore opening, generating the largest total pore volume and highest surface area. KOH activation, in contrast, generated a narrower micropore-dominated structure. This explains why the KOH-activated samples should not be considered inferior because of their lower BET surface area. For CO_2 capture, particularly under pressure-driven adsorption conditions, the decisive structural feature is not the maximum possible surface area but the fraction of pore volume located in the micropore range and the accessibility of those pores to CO_2. Recent work on pore-size-controlled biomass activated carbons has shown that samples with similar BET surface areas but different pore-size distributions can show substantially different CO_2 adsorption behavior, demonstrating that pore-size distribution must be evaluated independently from surface area [11].

Overall, the textural analysis demonstrates that sunflower pith is an effective precursor for producing high-surface-area, micropore-rich activated carbons. NaOH activation is more effective for maximizing BET surface area and total pore volume, whereas KOH activation produces a more favorable microporous architecture for CO_2 adsorption. This distinction provides the structural basis for the later adsorption results: the best-performing adsorbent is not the material with the highest BET area, but the one with the most suitable micropore architecture. The activation-agent comparison therefore highlights the main design principle of this work: biomass-derived activated carbons for CO_2 capture should be optimized through controlled micropore engineering, not through indiscriminate surface-area maximization.

3.3 Morphological structure of carbonized samples

SEM analysis shows that the sunflower-pith-derived activated carbons retain an open, low-density morphology inherited from the pith precursor, but the two alkali hydroxides modify this framework differently (Fig. 5). This interpretation is supported by the earlier sunflower-pith study of Baysal et al., where SEM/Micro-CT analysis showed that raw sunflower pith has a lamellar, flake-like network and that the carbonized sunflower-pith char retained this flake-like morphology with carbon flakes of approximately 200 nm thickness [8]. Therefore, the open morphology observed in the present AC samples should not be interpreted as a random fracture texture produced only during activation; it is partly inherited from the cellular/lamellar architecture of the original pith and then amplified by alkali-assisted pore development. In AC-2, the KOH-activated sample shows a wrinkled, porous, and relatively continuous carbon framework, suggesting that activation opened the char structure while preserving part of the original carbon skeleton. Similar behavior has been reported for KOH-activated sunflower-straw biochar, where SEM showed that activation made the surface rougher and produced a richer pore structure, while FTIR indicated that KOH activation changed both the surface chemistry and microstructure of sunflower-derived biochar [28].

In contrast, AC-4 appears more etched, irregular, and fragmented, which is consistent with the textural data showing that NaOH activation generated the highest BET surface area, largest total pore volume, and larger average pore diameter. A recent NaOH/KOH comparison on wood-derived carbons similarly reported slightly higher N_2 sorption and higher specific surface areas for NaOH-activated samples than for KOH-activated analogues, indicating that NaOH can produce stronger overall textural expansion in some lignocellulosic chars [19]. The SEM images alone cannot resolve micropores, so they should not be used as direct proof of the micropore fraction. However, they do support the broader mechanistic picture: both hydroxides strongly attack the sunflower-pith char, but KOH appears to preserve a more coherent porous carbon framework, whereas NaOH produces a more extensively etched and opened morphology. This interpretation is also consistent with recent discussions of biomass activation, where pore architecture is described as being controlled by activator infiltration, melting/diffusion, penetration depth, and interfacial reactions with biomass-derived carbon skeletons [20]. For CO_2 adsorption, the morphological difference should therefore be linked to the N_2 sorption results: the more open NaOH-derived morphology is consistent with higher total pore volume and pore widening, whereas the KOH-derived framework, although less expanded in total surface area, better retains the narrow micropore-rich structure required for strong CO_2 affinity. Recent CO_2-capture studies on K-based biomass activated carbons also show that high CO_2 uptake is associated with ultramicropore development rather than simply with the largest total surface area [15].

3.4 CO_2 adsorption performance

The CO_2 adsorption isotherms confirm that sunflower-pith-derived activated carbons are substantially more effective than the commercial activated carbon, particularly at elevated pressure (Fig. 6). At 8 bar and 25°C, the commercial activated carbon adsorbed only 4.58 mmol CO_2 g^{-1}, whereas all synthesized carbons showed markedly higher uptake. The best-performing sample was AC-2, the KOH-activated

carbon obtained from the 120 min carbonized char, with an uptake of 13.92 mmol g^{-1}. AC-4, although it possessed the highest BET surface area among all samples, adsorbed 10.87 mmol g^{-1}. This result is the central structure–performance finding of the study: CO_2 uptake does not scale simply with total BET surface area. Instead, adsorption is governed by the balance between accessible pore volume and the fraction of narrow micropores that provide strong adsorption potentials for CO_2.

The comparison between AC-2 and AC-4 is especially important. AC-4 had the highest BET surface area and total pore volume, indicating that NaOH activation produced the strongest overall textural expansion. However, AC-4 also had a larger average pore diameter and a lower micropore/total pore-volume ratio than AC-2. This suggests that part of the NaOH-generated surface area belongs to wider pores that contribute less strongly to CO_2 adsorption per unit pore volume. In contrast, AC-2 had a lower BET surface area but a higher micropore fraction and smaller average pore diameter, which are more favorable for CO_2 adsorption because the overlapping adsorption potentials from opposing pore walls enhance the interaction with the quadrupolar CO_2 molecule. This interpretation agrees with recent CO_2-capture studies showing that high adsorption capacity in biomass-derived activated carbons is associated with ultramicropore development rather than simply with maximum BET surface area. Dziejarski et al. reported that a KOH-activated biomass carbon achieved the highest CO_2 uptake among their samples because of extensive ultramicropore development, while a co-activated sample with favorable overall textural properties did not necessarily give the highest uptake [15]. Similarly, recent reviews emphasize that optimization of pore diameter and structure, not surface area alone, is crucial for improving CO_2 capture by biomass-derived activated carbons [3].

The commercial activated carbon provides a useful baseline for evaluating the synthesized materials. Although commercial carbons are often effective general-purpose adsorbents, the commercial sample used here had a much lower surface area, lower micropore volume, and larger average pore diameter than the sunflower-pith-derived carbons. Its lower CO_2 uptake therefore reflects not only lower total porosity but also less favorable pore-size matching for CO_2. The improvement is particularly clear at 8 bar: AC-2 adsorbed approximately three times more CO_2 than the commercial sample. This demonstrates that the sunflower-pith precursor, combined with alkali activation, generates a pore architecture more suitable for pressure-driven CO_2 adsorption than the commercial reference carbon.

The values in Table 5 should also be interpreted in terms of precursor, activation route, and pressure. At 8 bar and 25°C, AC-2 reached 13.92 mmol g^{-1}, which is higher than several biomass-derived activated carbons reported under similar elevated-pressure conditions, including Arundo donax-derived KOH-activated carbons with reported uptakes of 3.00-11.17 mmol g^{-1} and coconut-shell-derived activated carbon with 7.72 mmol g^{-1}. It is also higher than the unmodified H_3PO_4-activated eucalyptus carbon listed in the table, 10.12 mmol g^{-1}, but slightly lower than the ammonia-treated eucalyptus carbon, 14.06 mmol g^{-1}. This comparison shows that sunflower-pith-derived AC-2 is not merely better than the commercial carbon; it is competitive with high-performing biomass-derived adsorbents reported for

elevated-pressure CO_2 capture. The eucalyptus sample with the highest uptake likely benefits from additional nitrogen/amine-related surface modification or more favorable ultramicropore development, whereas the present AC-2 achieves comparable performance without post-synthetic nitrogen functionalization. That is an important practical advantage because it keeps the synthesis route simpler.

The pressure dependence further supports the pore-structure interpretation. At low pressure, the difference between samples prepared from 60 and 120 min carbonized chars was modest, especially for the NaOH-activated carbons. This indicates that the strongest adsorption sites, probably narrow micropores, are already populated early in the adsorption process. At higher pressure, however, the effect of carbonization time became more visible for KOH activation. Extending the carbonization time from 60 to 120 min increased the 8 bar CO_2 uptake of the KOH-activated carbon by approximately 23%. This suggests that the more completely carbonized precursor interacts more favorably with KOH during activation, producing not only strong low-pressure adsorption sites but also a larger accessible micropore volume that can be filled at elevated pressure. This distinction between low-pressure affinity and high-pressure capacity is consistent with recent biomass-carbon literature, where high-pressure CO_2 uptake is understood to benefit from both strong adsorption in narrow micropores and sufficient accessible pore volume [15, 29].

Temperature-dependent CO_2 adsorption of AC-2 further confirms the physisorptive and exothermic character of the adsorption process (Fig. 7). The uptake decreased as adsorption temperature increased, which is expected because higher temperature weakens the effective CO_2–surface interaction and reduces equilibrium adsorption. Similar behavior is widely reported for biomass-derived activated carbons. For example, recent olive-stone and almond-shell activated carbons showed reduced breakthrough time and adsorption performance at higher temperature, consistent with the exothermic nature of CO_2 adsorption [30]. A recent optimized date-palm-leaflet activated carbon also showed decreasing uptake with temperature, with reported capacities of 6.71 mmol g^{-1} at 0°C, 4.21 mmol g^{-1} at 25°C, and 2.6 mmol g^{-1} at 50°C [29]. Therefore, the temperature response of AC-2 is consistent with physical adsorption in microporous carbon rather than irreversible chemisorption.

Overall, the CO_2 adsorption results show that sunflower-pith-derived activated carbons are promising elevated-pressure CO_2 adsorbents. The best sample, AC-2, combines high uptake, a simple biomass-derived synthesis route, and a micropore-rich structure produced by KOH activation. The comparison with AC-4 demonstrates that maximizing BET surface area is not sufficient; excessive pore widening can reduce the fraction of adsorption-relevant micropores. The comparison table therefore supports the main conclusion of the work: sunflower pith can be converted into a competitive CO_2 adsorbent, but the activation strategy must be optimized for micropore architecture rather than total surface area alone.

For practical CO_2 capture, high adsorption capacity alone is not sufficient; the adsorbent must also retain its capacity during repeated adsorption–desorption cycles. In pressure-swing or vacuum-swing adsorption processes, the material is exposed repeatedly to CO_2 uptake and regeneration steps, and any

irreversible adsorption, pore blocking, framework degradation, or slow desorption can progressively reduce working capacity. Therefore, cyclic stability is an important indicator of whether the adsorption process is predominantly reversible physisorption and whether the pore network remains accessible after regeneration. Activated carbons are generally attractive in this respect because their rigid carbon framework, chemical stability, and relatively low adsorption enthalpy allow regeneration by pressure reduction or mild thermal/vacuum treatment [15, 31].

To evaluate the recyclability of the best-performing sample, AC-2 was subjected to 10 consecutive CO_2 adsorption–desorption cycles at 25°C, with desorption carried out under vacuum at 0.01 mbar (Fig. 8). The uptake retention remained very high throughout cycling, decreasing only from 100.0% in the first cycle to 97.8% after the tenth cycle. This corresponds to a total capacity loss of only 2.2%, while the average retention over all cycles was 98.8%. The small cycle-to-cycle variations, such as the slight increase from cycle 3 to cycle 4, are within the expected range of experimental fluctuation and do not indicate continuous deactivation. The high retention confirms that CO_2 adsorption on AC-2 is largely reversible under the applied regeneration conditions and that the microporous network remains stable and accessible during repeated use.

This stability is consistent with recent reports on biomass-derived activated carbons. Dziejarski et al. reported adsorption–desorption cycling of KOH- and $K_2C_2O_4$-activated biomass carbons at 25°C for 20 cycles and observed no measurable capacity loss, with a maximum standard deviation of approximately 0.09 mmol g^{-1}, which they attributed to stable physisorption within persistent ultramicropores [15]. Moussa et al. also evaluated olive-stone-derived porous carbons over six adsorption–desorption cycles under CO_2/N_2 gas mixtures and reported that KOH-activated samples maintained almost complete stability, whereas some metal-modified samples showed slight capacity decreases in later cycles [31]. Compared with these reports, the 97.8% retention of AC-2 after 10 cycles demonstrates competitive regeneration stability and supports the conclusion that the sunflower-pith-derived activated carbon behaves as a robust physisorbent. Although longer cycling tests under mixed-gas and humid conditions would be useful for future process validation, the present 10-cycle vacuum-regeneration test provides strong initial evidence for the reusability of AC-2 in repeated CO_2 capture operation.

3.5 Isosteric heat of adsorption and adsorption energetics

The adsorption energetics of AC-2 were evaluated from CO_2 adsorption isotherms collected at 298, 318, and 338 K, because this sample showed the highest uptake among the synthesized activated carbons. The CO_2 uptake decreased with increasing adsorption temperature, confirming that adsorption is exothermic. The isotherms were first treated using a Langmuir-based surface-coverage analysis. From the linearized P/m versus P plots, the monolayer adsorption masses were calculated as 27.47 mg at 298 K, 24.50 mg at 318 K, and 23.31 mg at 338 K (Figure S3). These monolayer values were then used to convert the adsorption data into surface coverage, θ, as a function of pressure (Figure S4).

The isosteric heat was calculated from Clausius-Clapeyron plots of ln P versus 1/T at fixed surface coverage. For θ = 0.80, θ = 0.75, and θ = 0.70, the adsorption enthalpies were ΔH = -13.88, -8.73, and −6.55 kJ mol^{-1}, respectively. These can also be expressed as positive heat-of-adsorption magnitudes Q_{st}. The negative sign of ΔH confirms the exothermic nature of CO_2 adsorption on AC-2, while the low magnitudes indicate that the interaction is dominated by physical adsorption rather than chemisorption.

These values are lower than many recent values reported for biomass-derived activated carbons. Kuloglija et al. calculated isosteric heats of adsorption for KOH-activated pine- and birch-derived carbons using fixed loading, reporting values from 16.6 to 29.4 kJ mol^{-1}, which they described as consistent with physisorption of CO_2 on activated carbons [14]. Dziejarski et al. reported higher Q_{st} values of 26–36 kJ mol^{-1} for K-based biomass activated carbons and described them as strong physisorption; their simulations also linked enhanced CO_2 affinity to sub-nanometer pores and carbonyl-rich surfaces [15]. Al-Ghurabi et al. reported an even higher value of 35 kJ mol^{-1} at low CO_2 loading for optimized date-palm-waste activated carbon, attributing it to energetically heterogeneous nanopore sites and preferential micropore filling [29]. Compared with these recent studies, AC-2 shows weaker apparent adsorption energetics, even though it has high CO_2 uptake at elevated pressure.

This comparison suggests that AC-2 does not achieve its high 8 bar CO_2 capacity because of unusually strong binding sites. Instead, its performance is mainly associated with pressure-driven filling of its accessible microporous structure. This is consistent with the textural results: AC-2 has a high micropore fraction and a smaller average pore diameter than the NaOH-activated sample, but its calculated adsorption enthalpy remains low. In practical terms, this can be advantageous. Materials with higher Q_{st} may show stronger low-pressure affinity and selectivity, but they can require more energy for regeneration. The relatively low Q_{st} values of 13.88, 8.73, and 6.55 kJ mol^{-1} suggest that CO_2 adsorbed on AC-2 should be releasable by pressure reduction, vacuum, or mild heating. Thus, AC-2 should be described as a high-capacity, pressure-responsive physisorbent rather than a strongly binding chemisorptive adsorbent.

Structure–performance descriptor for CO_2 uptake

The CO_2 adsorption results show that the sunflower-pith-derived activated carbons cannot be evaluated using BET surface area alone. Although AC-4 exhibited the highest BET surface area and micropore volume, AC-2 delivered the highest CO_2 uptake. This inversion indicates that adsorption performance is not controlled simply by the total amount of internal surface generated during activation, but by how effectively that porosity is distributed within CO_2-accessible micropores. In other words, the relevant structural factor is not only the quantity of micropore volume, but also the degree of confinement imposed on CO_2 molecules by the pore walls. This observation motivated the use of a simple textural descriptor to examine the combined effect of micropore volume and average pore diameter on CO_2 adsorption.

As a first approximation, micropore volume was normalized by pore diameter. This approach has a direct geometrical basis. For idealized slit-like or cylindrical pores, internal surface area scales approximately with pore volume divided by pore width. Therefore, V_{micro}/d_{avg} already contains an implicit surface-area contribution and may be interpreted as a rough proxy for micropore-associated internal surface area. This is important because the total BET surface area is not necessarily equivalent to CO_2-effective surface area. BET area can include contributions from wider micropores and small mesopores, which increase total surface area but do not necessarily provide the strongest adsorption sites for CO_2. Therefore, the descriptor was constructed around the microporous domain rather than the total BET surface area.

However, V_{micro}/d_{avg} alone does not fully represent the strong influence of pore-size confinement. CO_2 adsorption in narrow carbon micropores is enhanced by the overlap of adsorption potentials from opposing pore walls. As the pore width increases, this overlap weakens nonlinearly, reducing the adsorption affinity of the pore even if the pore still contributes to total surface area or total pore volume. Therefore, the descriptor was generalized as:

$$D_n = \frac{V_{micro}}{d_{avg}^{n}}$$

where n is an empirical confinement-sensitivity exponent. For the sunflower-pith activated carbons, the 8 bar CO_2 uptake was best represented by n = 3, giving the descriptor $D_3=V_{micro}/d_{avg}^{3}$ (Fig. 9). This descriptor correctly identifies AC-2 as the most favorable adsorbent and explains why AC-4, despite having the highest BET surface area and micropore volume, shows lower CO_2 uptake: its larger average pore diameter weakens the confinement contribution. Therefore, the descriptor number is not presented as a universal adsorption equation, but as a confinement-weighted micropore descriptor that captures the main structure–performance trend within this internally consistent synthesis series.

The same analysis was repeated using the 1 bar CO_2 uptake values obtained from the adsorption isotherms. At 1 bar, the best mathematical exponent increased to approximately n = 5, although n = 3 still produced a reasonable correlation. This pressure dependence is physically meaningful. At low pressure, adsorption occurs preferentially in the strongest adsorption sites, namely narrow micropores and ultramicropores where wall-potential overlap is most significant. Under these conditions, pore width exerts a stronger effect on uptake, and a larger exponent is expected. At higher pressure, once the strongest adsorption sites are progressively occupied, additional micropore volume contributes more strongly to total capacity, and the pore-width penalty becomes less dominant. Thus, the exponent n should be viewed as a condition-dependent confinement parameter rather than as a fixed material constant.

This interpretation is consistent with recent literature. Dan et al. investigated PET-derived activated carbons prepared by microwave activation and showed that activation time strongly affects textural properties and CO_2 uptake. Their study reported that the optimum PET-derived carbon was not simply

the most extensively activated material, but the material with the most favorable balance of micropore volume, pore width, and CO_2 uptake [32]. When their reported CO_2-derived micropore volume and characteristic pore width were examined using the related descriptor $W_{0,CO2}/L_0^n$, a strong pore-width-weighted correlation was obtained. This supports the conclusion that CO_2 uptake in activated carbons is governed by the combined effect of micropore volume and pore-size confinement, rather than by total surface area alone.

Table 5
Comparison of the adsorption capacity of the synthesized AC samples at 8 bars and 25°C

Adsorbent	**Activation / treatment**	**CO_2 uptake (mmol g^{-1})**	**Reference**
Eucalyptus wood carbon	H_3PO_4, unmodified	10.12	[33]
Eucalyptus wood carbon	H_3PO_4 + NH_3 at 400°C	3.96	[33]
Eucalyptus wood carbon	H_3PO_4 + NH_3 at 800°C	14.06	[33]
Arundo donax carbon	KOH 0:1	3.00	[34]
Arundo donax carbon	KOH 1:1	5.93	[34]
Arundo donax carbon	KOH 2:1	7.12	[34]
Arundo donax carbon	KOH 3:1	11.17	[34]
Coconut shell carbon	Steam	7.72	[35]
Commercial AC	Coal-based commercial AC	4.58	This work
AC-2	Sunflower pith, KOH	13.92	This work
AC-4	Sunflower pith, NaOH	10.87	This work

A second comparison was made using the olive-stone-derived carbon study by Moussa et al. In that work, CO_2 uptake was measured at 0°C and 1 bar for olive-stone-based carbons. For that dataset, the descriptor fits with an n number of 0.5. This does not contradict the present analysis. Instead, it shows that temperature and adsorption energy also affect the number. In the olive-stone study, CO_2 adsorption was performed at 0°C, meaning that it is much easier to adsorb under these conditions [31].

Taken together, these comparisons show that the exponent n should not be treated as a universal number. It can vary with pressure, temperature, precursor structure, activation method, and the pore-volume metric used. If the pore-volume term is a broad N_2-derived micropore volume, a stronger pore-width penalty may be required because not all micropores contribute equally to CO_2 adsorption. If the pore-volume term is already CO_2-derived or restricted to ultramicropores, a weaker additional pore-width penalty may be sufficient. Activation chemistry and precursor structure can further modify this relationship by affecting pore accessibility, pore tortuosity, surface polarity, residual inorganic species, and the distribution of oxygen-containing functional groups. Therefore, this equation should be

considered a semi-quantitative structure performance descriptor rather than a predictive universal model.

Despite these limitations, the descriptor analysis strengthens the mechanistic interpretation of the present work. The superior performance of AC-2 is not an accidental consequence of high surface area, nor can it be explained by total pore volume alone. Instead, AC-2 provides the most favorable balance between micropore volume and pore confinement. The descriptor provides a compact way to visualize this balance and to compare related activated carbons within a controlled synthesis series. Its value is not in replacing adsorption isotherms, but in offering a first-pass screening metric for identifying activated carbons in which the generated porosity is not only abundant, but also appropriately confined for CO_2 adsorption.

4. Conclusion

Sunflower pith was demonstrated as an effective low-cost agricultural precursor for producing high-surface-area activated carbons for CO_2 capture. Carbonization converted the naturally cellular pith structure into a carbon-rich framework, while increasing carbonization temperature and residence time progressively lowered char yield through dehydration, devolatilization, cleavage of oxygenated/aliphatic moieties, and development of a more carbonized aromatic structure. Although the directly carbonized biochars retained only limited surface area, they provided a suitable reactive carbon framework for subsequent alkali activation. Chemical activation transformed these low-surface-area chars into highly porous activated carbons, increasing the BET surface area from below 6 m^2g^{-1} for the biochars to above 2000 m^2g^{-1} for all synthesized activated carbons.

The key finding of this work is that CO_2 adsorption performance was not governed by BET surface area alone. NaOH activation generated the largest total surface area and pore volume, with AC-4 reaching 2948 m^2g^{-1}, but this did not translate into the highest CO_2 uptake. Instead, the KOH-activated AC-2 showed the best adsorption performance, reaching 13.92 mmol g^{-1} at 25°C and 8 bar, substantially exceeding both the commercial activated carbon and the NaOH-activated analogues. This result demonstrates that the quality of the pore architecture is more important than simple surface-area maximization. The superior behavior of AC-2 is attributed to its more favorable balance of micropore volume, micropore fraction, and smaller average pore diameter, which provides stronger confinement for CO_2 while maintaining sufficient accessible pore volume.

The comparison between KOH and NaOH activation, therefore, provides a clear mechanistic design message. NaOH activation appears to promote more extensive pore widening and total pore development, whereas KOH activation produces a more CO_2-effective microporous network in sunflower-pith-derived carbon. The inversion between BET surface area and CO_2 uptake highlights the importance of targeted micropore engineering, especially for adsorbents intended for pressure-swing or vacuum-swing CO_2 capture. Temperature-dependent adsorption measurements further confirmed the exothermic

and predominantly physical nature of CO_2 adsorption, while the cyclic adsorption–desorption test of AC-2 showed high regeneration stability, retaining 97.8% of its initial uptake after 10 cycles under vacuum desorption. These results indicate that AC-2 combines high capacity, reversible adsorption, and promising structural stability during repeated use.

To quantify this structure–performance relationship, a confinement-weighted micropore descriptor, $D_n=V_{micro}/d_{avg}^3$ was introduced. Although not proposed as a universal predictive equation, the descriptor captured the internal trend of the sunflower-pith-derived carbons and showed that the superior uptake of AC-2 arises from the combined effect of micropore volume and pore-size confinement. This analysis provides a practical screening concept for comparing related activated carbons where BET surface area alone fails to explain CO_2 adsorption behavior.

Overall, this study establishes sunflower pith as a promising biomass precursor for regenerable CO_2-capture activated carbons and shows that alkali activation chemistry can be used to tune the pore network toward CO_2-selective confinement. The work also emphasizes that future development of biomass-derived activated carbons should move beyond reporting high BET surface area as the primary performance indicator. Instead, pore-size distribution, micropore fraction, average pore diameter, adsorption energetics, and cyclic working capacity should be considered together.

Declarations

Author Contribution

S.S.H. performed the experiments, analyzed the experimental data, and wrote the first draft of the manuscript. A.Y. supervised the study, edited the manuscript, expanded the scientific discussion, interpreted the adsorption and textural-property results, and revised the manuscript for intellectual content. Both authors reviewed and approved the final manuscript.

References

1. Deng, Z., Zhu, B., Davis, S.J., Ciais, P., Guan, D., Gong, P., Liu, Z.: Global carbon emissions and decarbonization in 2024. Nat. Reviews Earth Environ. **6**, 231–233 (2025)
2. Wang, P., Robinson, A.J., Papadokonstantakis, S.: Prospective techno-economic and life cycle assessment: a review across established and emerging carbon capture, storage and utilization (CCS/CCU) technologies. Front. Energy Res. **12**, 1412770 (2024)
3. Kundu, S., Khandaker, T., Anik, M.A.M., Hasan, M.K., Dhar, P.K., Dutta, S.K., Latif, M.A., Hossain, M.S.: A comprehensive review of enhanced CO_2 capture using activated carbon derived from biomass feedstock. RSC Adv. (2024). 10.1039/D4RA04537H
4. Quan, C., Zhou, Y., Wang, J., Wu, C., Gao, N.: Biomass-based carbon materials for CO_2 capture: A review. J. CO_2 Utilization. **68**, 102373 (2023)

5. Abuelnoor, N., AlHajaj, A., Khaleel, M., Vega, L.F.: Abu-Zahra, Activated carbons from biomass-based sources for CO_2 capture applications. Chemosphere. **282**, 131111 (2021)
6. Khosrowshahi, M.S., Ghasemi, S.S., Safdari, M., et al.: Natural products derived porous carbons for CO_2 capture. Adv. Sci. **10**, 2304289 (2023)
7. Oschatz, M., Antonietti, M.: A search for selectivity to enable CO_2 capture with porous adsorbents. Energy Environ. Sci. **11**, 57–70 (2018)
8. Baysal, M., Bilge, K., Yılmaz, B., Papila, M., Yürüm, Y.: Preparation of high surface area activated carbon from waste-biomass of sunflower piths: Kinetics and equilibrium studies on dye removal. J. Environ. Chem. Eng., (2018)
9. Rambhatla, N.: Biomass pyrolysis for biochar production: Study of kinetics and physicochemical characteristics. Results Eng. **25**, 103716 (2025)
10. Vilas-Boas, A.C.M., et al.: Valorisation of residual biomass by pyrolysis. Sustainable Energy Fuels. **8**, 637–649 (2024)
11. Sathyabama, K., et al.: Effect of Pyrolysis Temperature on the Physicochemical Properties of Biochar. Biochar, (2025)
12. Hoang, T.-D., Liu, Y., Le, M.T.: Synthesis and Characterization of Biochars and Activated Carbons Derived from Various Biomasses. Sustainability. **16**(13), 5495 (2024). 10.3390/su16135495
13. Tonu, N.T., Kundu, S., Islam, M.M., Dhar, P.K., Khandaker, T., Anik, M.A.A.M., Dutta, S.K., Hasan, M.K., Hossain, M.S.: Fabrication of waste biomass-derived KOH activated carbon for enhanced CO_2 capture. New J. Chem. **48**, 20212–20224 (2024). 10.1039/D4NJ04495A
14. Kuloglija, S., et al.: Isotherms and kinetics of CO_2 adsorption on biochar-based activated carbon for sustainable climate solutions. Sep. Purif. Technol., (2025)
15. Dziejarski, B., Serafin, J., Hernández-Barreto, D.F., Naumovska, E., Sreńscek-Nazzal, J., Klomkliang, N., Tam, E., Krzyżyńska, R., Andersson, K., Knutsson, P.: Tailoring highly surface and microporous activated carbons from biomass via KOH, $K_2C_2O_4$ and KOH/$K_2C_2O_4$ activation for efficient CO_2 capture and CO_2/N_2 selectivity. Chem. Eng. J. **524**, 169677 (2025). 10.1016/j.cej.2025.169677
16. Durán-Jiménez, G., Rodriguez, J., Stevens, L., Kostas, E.T., Dodds, C.: Microwave pyrolysis of waste biomass and synthesis of micro-mesoporous activated carbons: The role of textural properties for CO_2 and textile dye adsorption. Chem. Eng. J. **493**, 150926 (2024). 10.1016/j.cej.2024.150926
17. Liu, P., Sun, S., Huang, S., Wu, Y., Li, X., Wei, X., Wu, S.: KOH Activation Mechanism in the Preparation of Brewer's Spent Grain-Based Activated Carbons. Catalysts. **14**(11), 814 (2024). 10.3390/catal14110814
18. Lillo-Ródenas, M.A., Cazorla-Amorós, D., Linares-Solano, A.: Understanding chemical reactions between carbons and NaOH and KOH: An insight into the chemical activation mechanism. Carbon. **41**(2), 267–275 (2003)
19. Dobele, G., Dizhbite, T., Volperts, A., Andersone, A., Telysheva, J., Rossinskaja, G.: Thermochemical Activation of Wood with NaOH, KOH and H_3PO_4 for the Synthesis of Nitrogen-Doped Nanoporous Carbon for Oxygen Reduction Reaction. Molecules. **29**(10), 2238 (2024)

20. Wu, W., Wang, Y., Hu, X.: Mass transfer driven pore engineering of activated carbon from the activation of biomass. Green Chem. **28**, 3486–3503 (2026)
21. Mochizuki, Y., et al.: Pore properties and CO_2 adsorption performance of porous carbon materials prepared from biomass and coal. Carbon Trends, (2025)
22. Marangon, A., et al.: Comparison of different activation methods for activated carbon production from bamboo biomass. Carbon Capture Science & Technology (2025)
23. Asmaly, H.A., et al.: Enhanced CO_2 capture using sustainable biomass-derived activated carbon. Carbon Capture Science & Technology (2026)
24. Bandani, M., et al.: Preparation and characterization of low-cost chemically activated porous carbon adsorbents from Parrotia persica wood for CO_2/N_2 separation. Sci. Rep., (2026)
25. Siemak, J., et al.: Activated carbon for CO_2 adsorption from avocado seeds using sodium hydroxide activation. Materials. **17**, 4157 (2024)
26. Mohamed, S.N., Saleh, et al.: Enhanced CO_2 capture using KOH-functionalized oil palm ash-derived adsorbents. Discover Appl. Sci., (2025)
27. Wang, Q., Li, T., Tian, H., Zou, D., Zeng, J., Chen, S., Xie, H., Zhou, G.: Effect of pore size distribution of biomass activated carbon on CO_2 adsorption. J. Chem. Technol. Biotechnol. **99**(5), 1148–1156 (2024)
28. Chang, S., Wang, L., Yao, L.: Properties of Sunflower Straw Biochar Activated Using Potassium Hydroxide. Molecules. **30**(6), 1332 (2025)
29. Al-Ghurabi, E.H., Boumaza, M.M., Al-Masry, W., Asif, M.: Optimizing the synthesis of nanoporous activated carbon from date-palm waste for enhanced CO_2 capture. Sci. Rep. **15**, 17132 (2025)
30. Rahimi, V., et al.: Evaluating the performance of carbon-based adsorbents fabricated from renewable biomass precursors for post-combustion CO_2 capture. Sep. Purif. Technol., (2024)
31. Moussa, M., Bohli, T., Pevida, C., Querejeta, N., Ouederni, A.: Valorization of Olive Stone Biomass into Graphitic-Like Carbon for Cyclic and Selective CO_2 Adsorption Under Postcombustion Conditions. Environ. Eng. Sci. **43**, 110–122 (2026)
32. Dan, E., McCue, A.J., Dionisi, D., Fernández Martín, C.: Towards low-cost and sustainable activated carbon production: Influence of microwave activation time on yield and CO_2 uptake of PET-derived adsorbents. J. CO_2 Utilization. **83**, 102807 (2024). 10.1016/j.jcou.2024.102807
33. Heidari, A., Younesi, H., Rashidi, A., Ghoreyshi, A.A.: Evaluation of CO2 adsorption with eucalyptus wood based activated carbon modified by ammonia solution through heat treatment. Chem. Eng. J. **254**, 503–513 (2014)
34. Singh, G., Kim, I.Y., Lakhi, K.S., Srivastava, P., Naidu, R., Vinu, A.: Single step synthesis of activated bio-carbons with a high surface area and their excellent CO2 adsorption capacity, Carbon, **116**, pp. 448–455, (2017)
35. Singh, V.K., Kumar, E.A.: Thermodynamic analysis of single-stage and single-effect two-stage adsorption cooling cycles using indigenous coconut shell based activated carbon-CO2 pair. Int. J.

Refrig. **84**, 238–252 (2017)

Figures

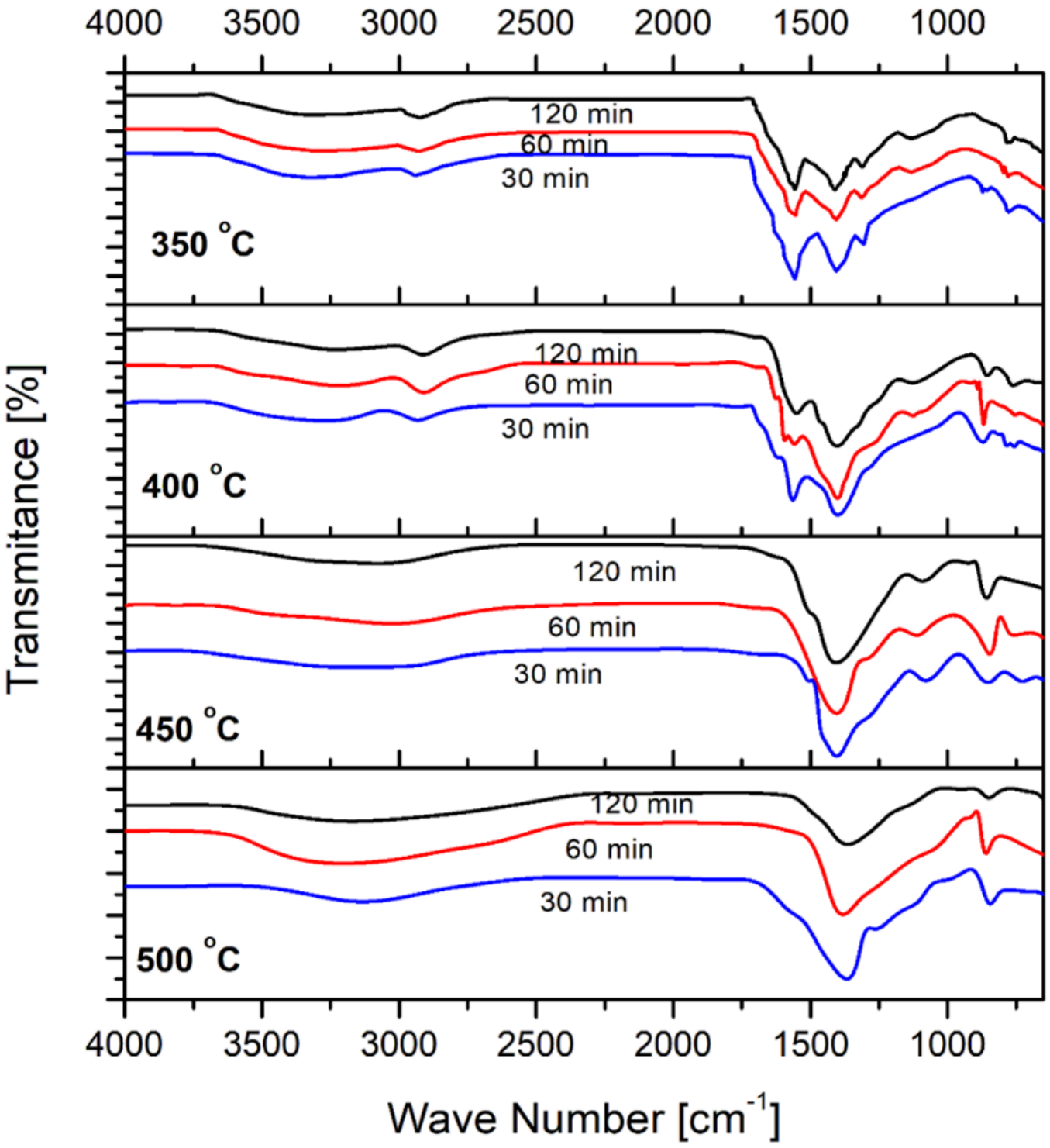

Figure 1

FTIR spectra for the biochar samples

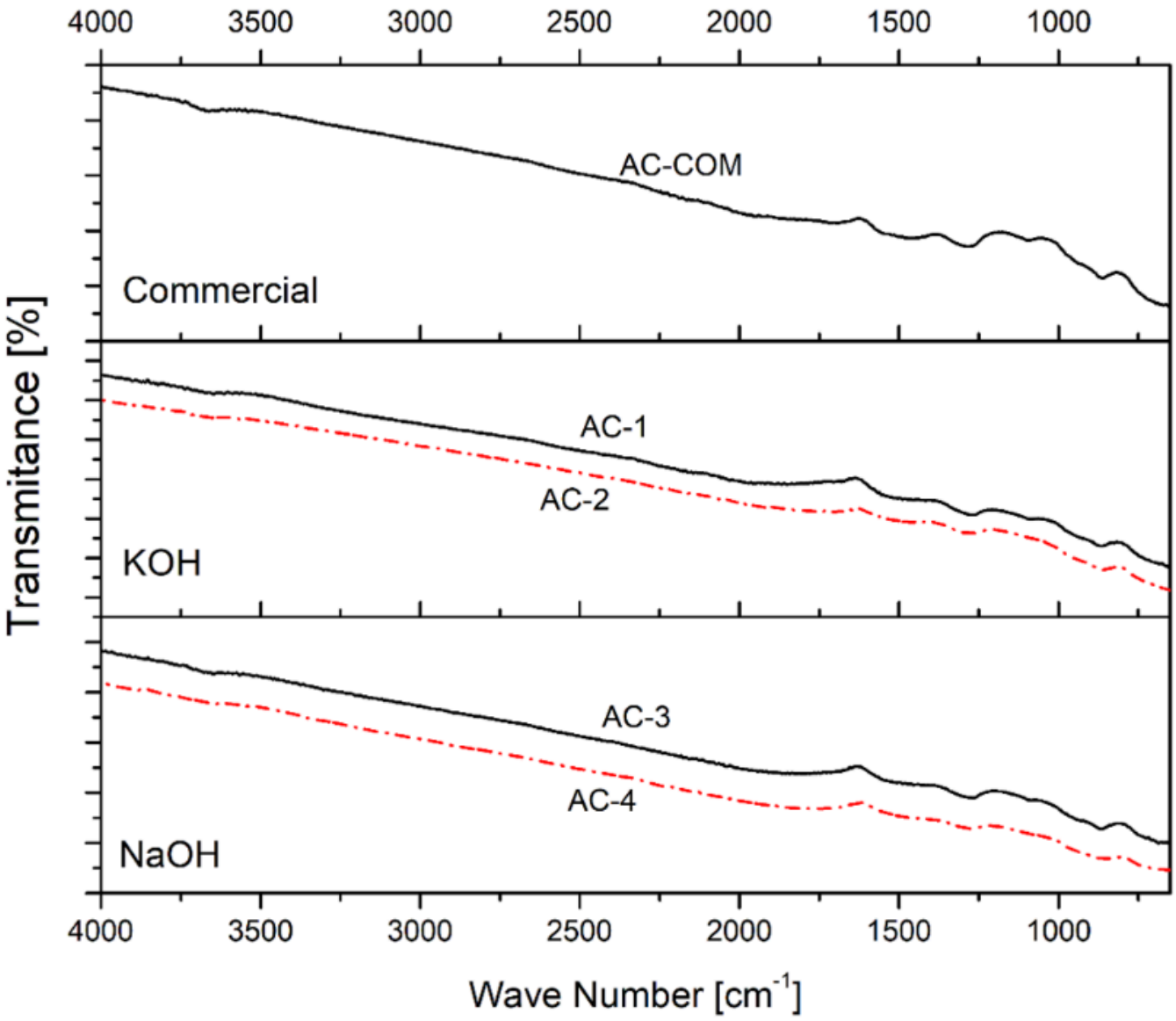

Figure 2

FTIR spectra for the activated samples

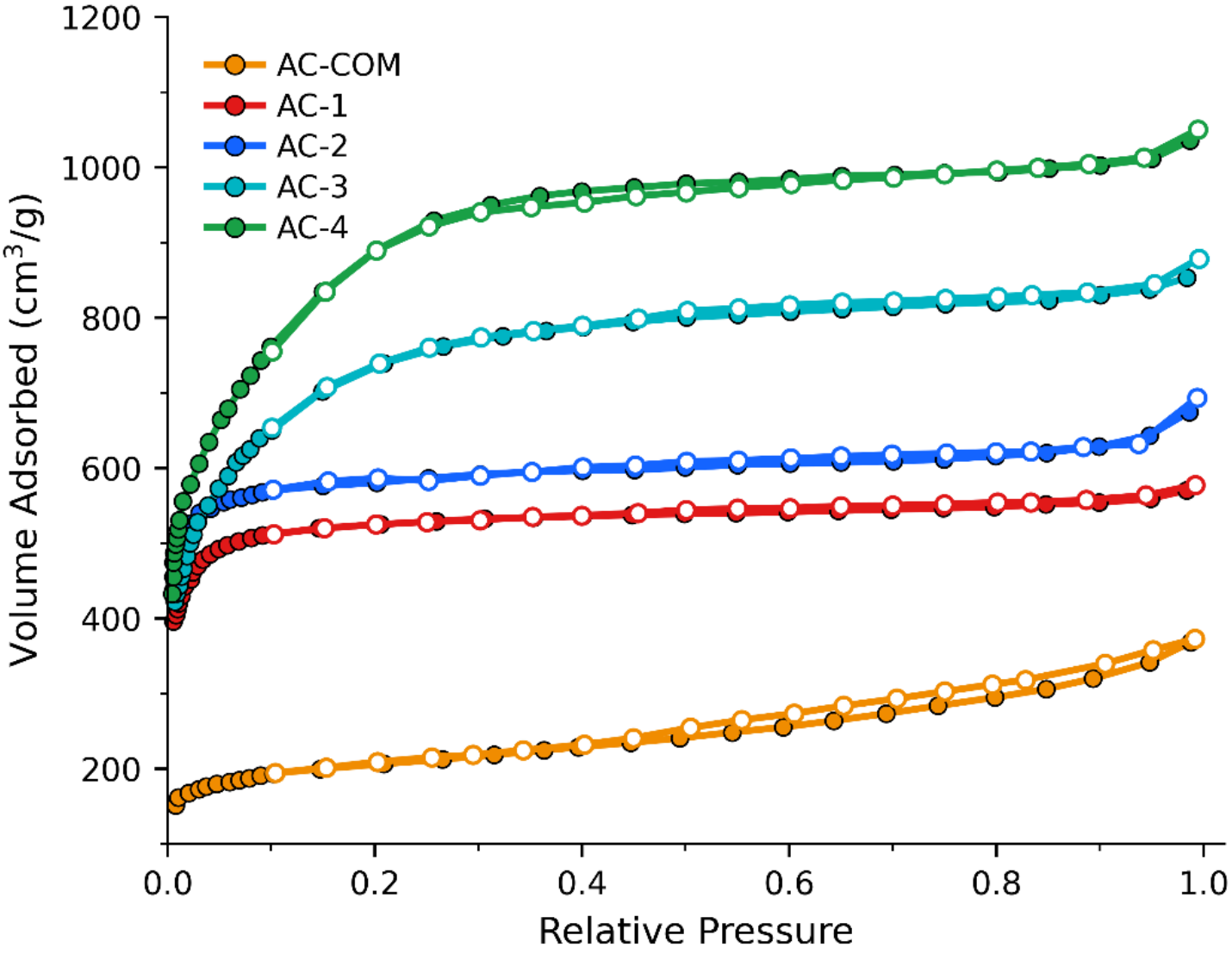

Figure 3

N_2 adsorption–desorption isotherms for the activated samples

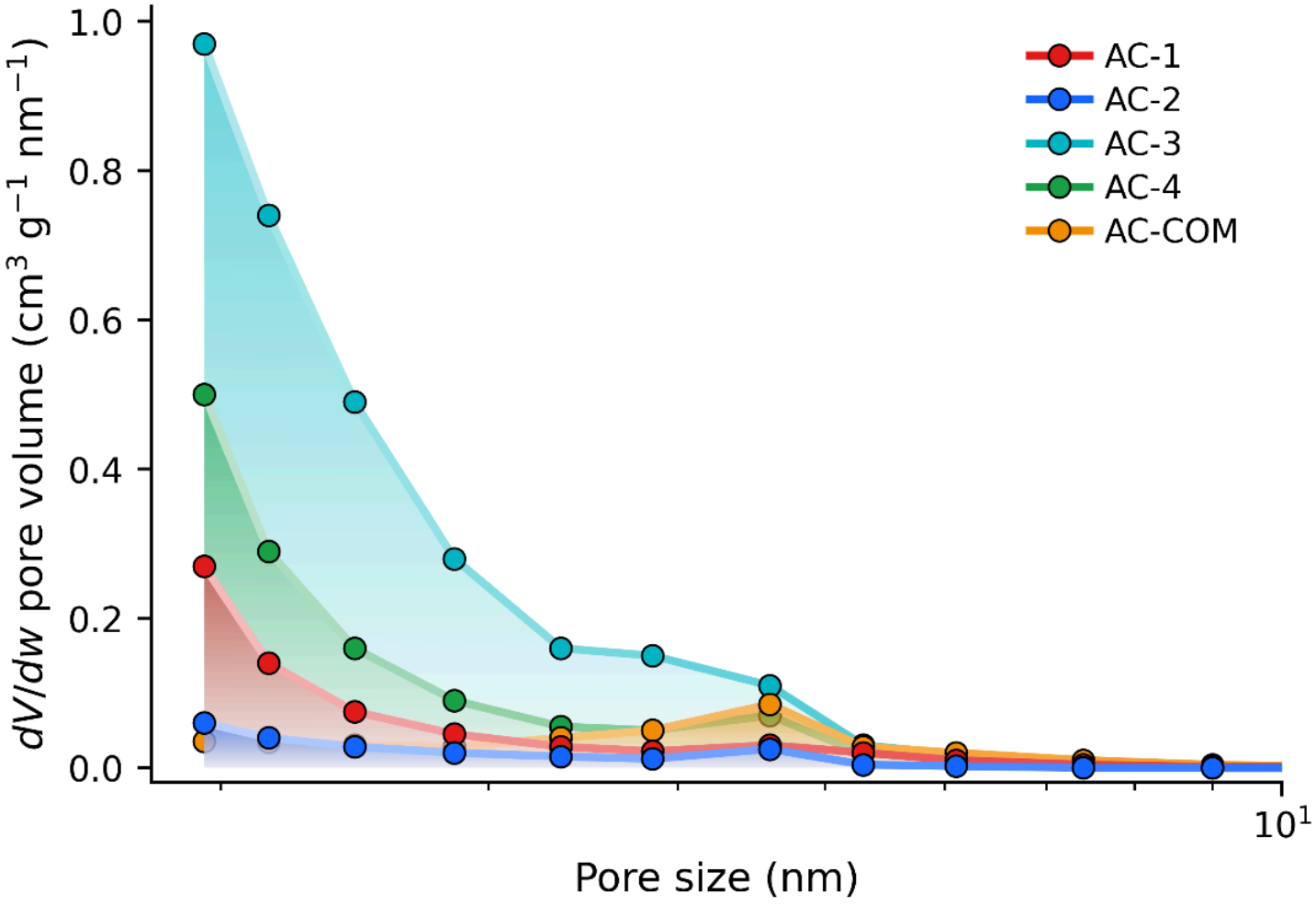

Figure 4

Pore size distribution of the activated samples

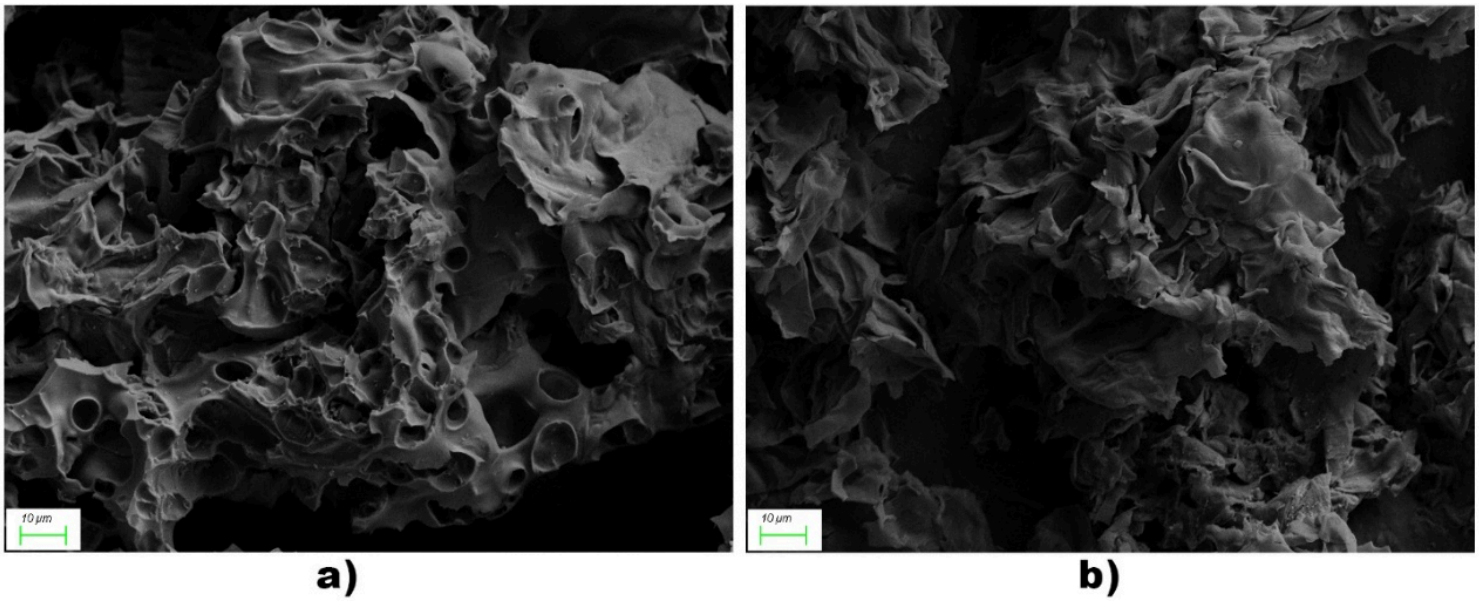

Figure 5

SEM images of a) AC-2, b) AC-4

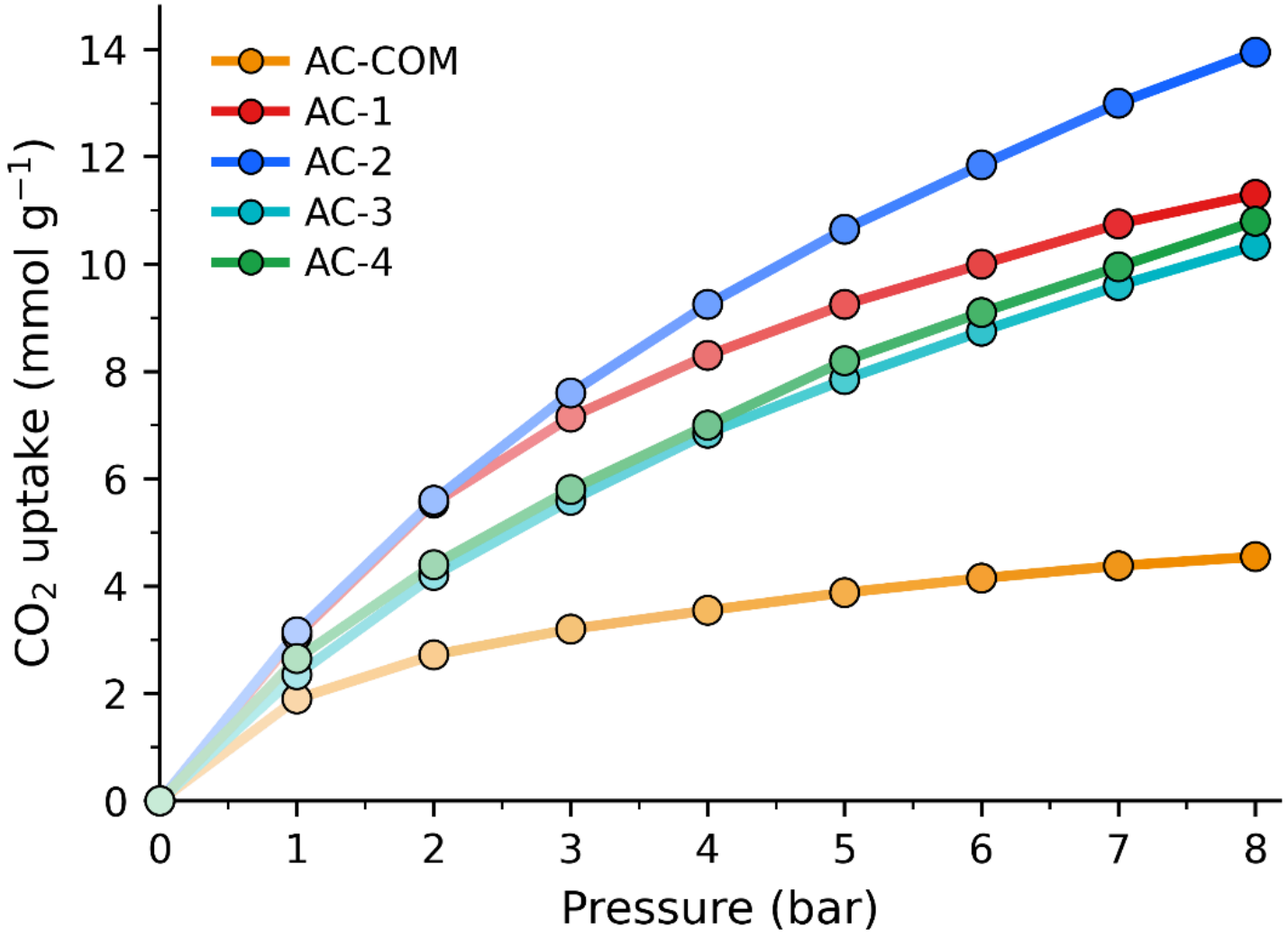

Figure 6

CO_2 adsorption isotherms on AC samples

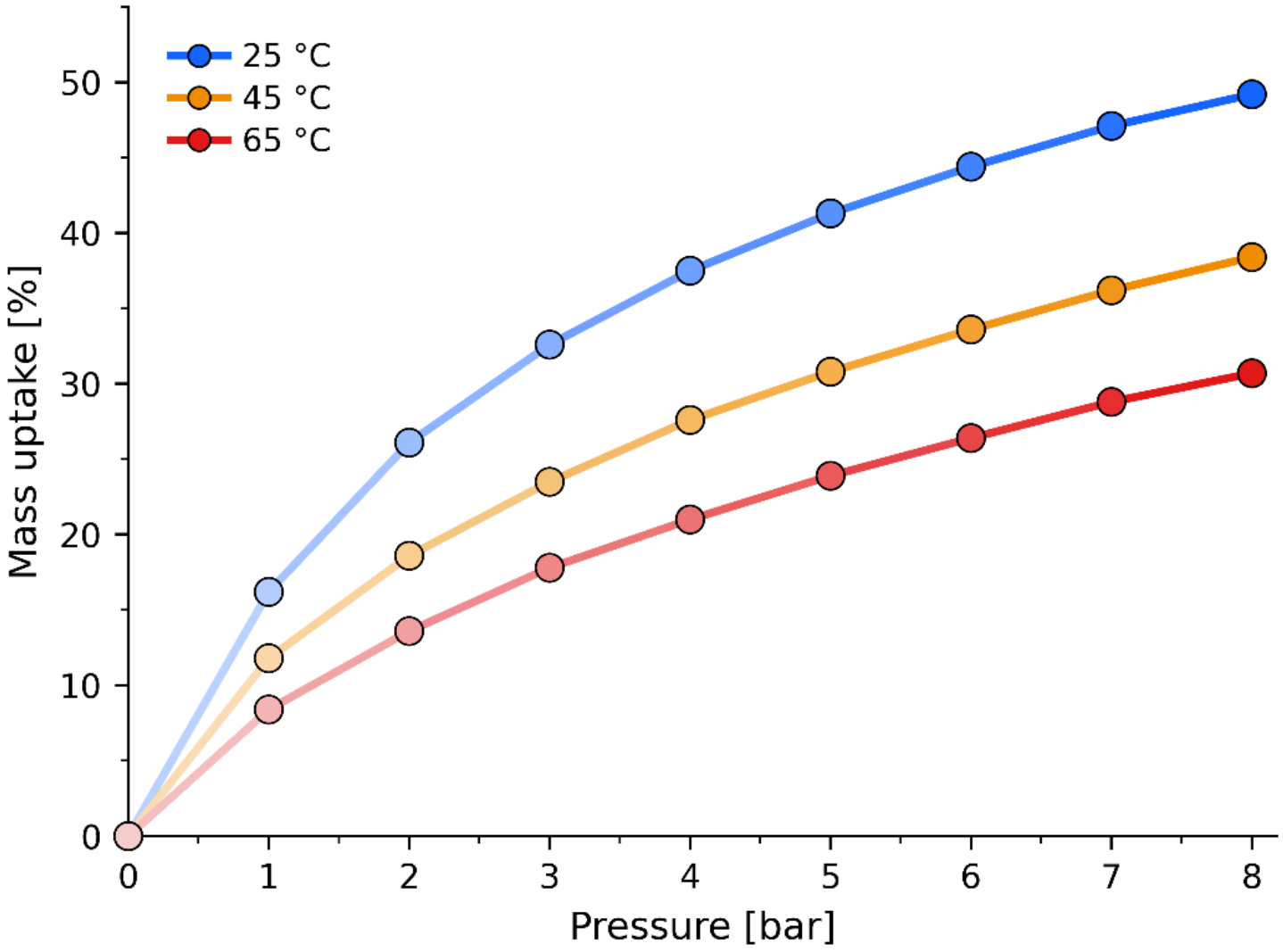

Figure 7

CO_2 adsorption isotherms on AC-2 at different temperatures

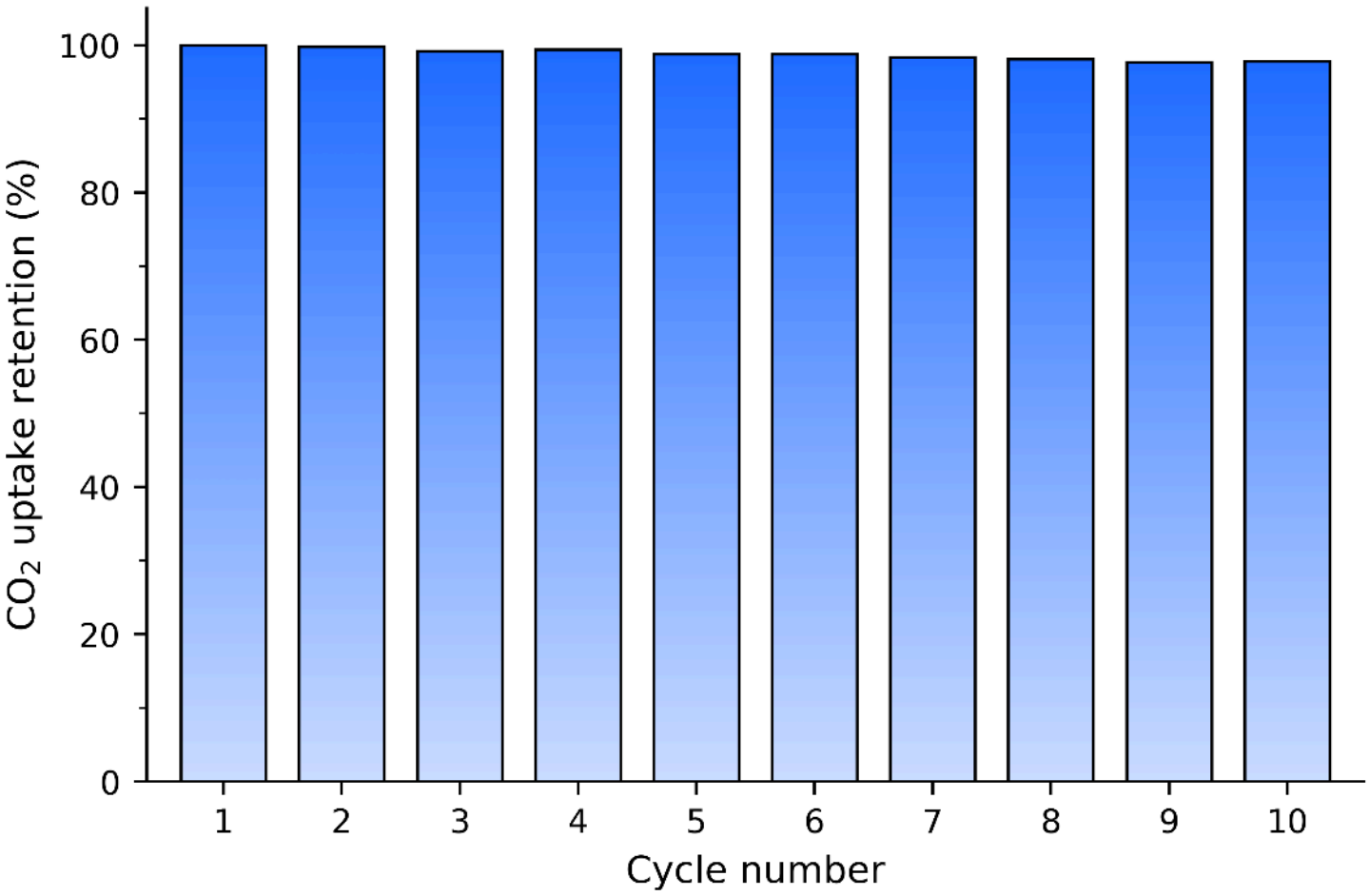

Figure 8

Recyclability performance of AC-2

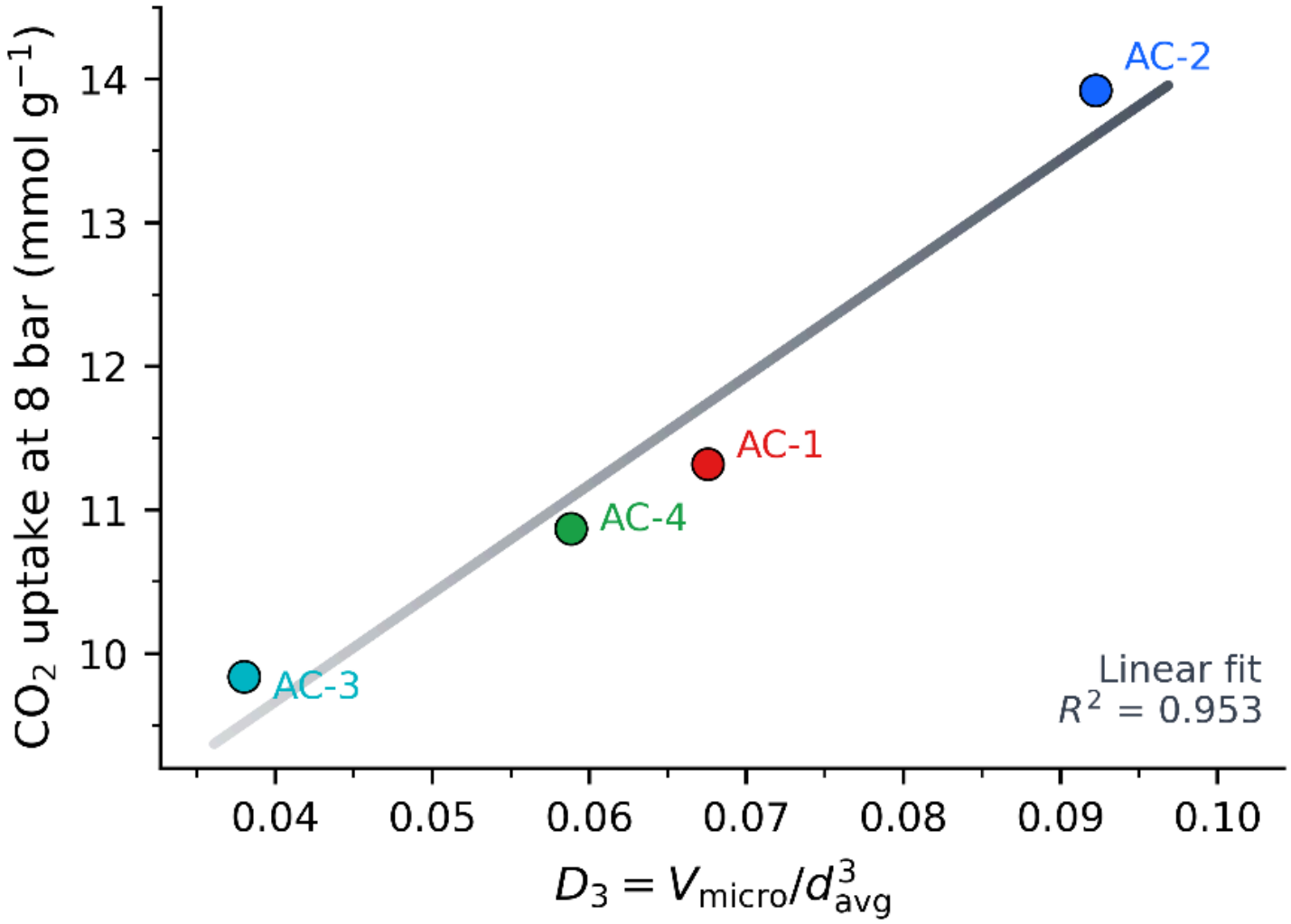

Figure 9

Descriptor fit of sunflower-pith AC at 8 bar

Supplementary Files

This is a list of supplementary files associated with this preprint. Click to download.

- SunflowerPithSI.docx